Available online at www.sciencedirect.com
SCIENCE DIRECT®
Remote Sensing of Environment 88 (2003) 170–186
Remote Sensing of Environment
www.elsevier.com/locate/rse

High spatial resolution spectral mixture analysis of urban reflectance

Christopher Small*

Lamont Doherty Earth Observatory, Columbia University, Palisades, NY 10964 USA

Received 9 May 2002; received in revised form 17 January 2003; accepted 22 April 2003

Abstract

This study uses IKONOS imagery to quantify the combined spatial and spectral characteristics of urban reflectance in 14 urban areas worldwide. IKONOS 1-m panchromatic imagery provides a detailed measure of spatial variations in albedo while IKONOS 4-m multispectral imagery allows the relative contributions of different materials to the spectrally heterogeneous radiance field to be determined and their abundance to be mapped. Spatial autocorrelation analyses indicate that the characteristic scale of urban reflectance is consistently between 10 and 20 m for the cities in this study. Spectral mixture analysis quantifies the relative contributions of the dominant spectral endmembers to the overall reflectance of the urban mosaic. Spectral mixing spaces defined by the two low-order principal components account for 96% to 99% of image variance and have a consistent triangular structure spanned by high albedo, low albedo and vegetation endmembers. Spectral mixing among these endmembers is predominantly linear although some nonlinear mixing is observed along the gray axis spanning the high and low albedo endmembers. Inversion of a constrained three-component linear mixing model produces stable, consistent estimates of endmember abundance. RMS errors based on the misfit between observed radiance vectors and modeled radiance vectors (derived from fraction estimates and image endmembers) are generally less than 3% of the mean of the observed radiance. Agreement between observed radiance and fraction estimates does not guarantee the accuracy of the areal fraction estimates, but it does indicate that the three-component linear model provides a consistent and widely applicable physical characterization of urban reflectance. Field validated fraction estimates have applications in urban vegetation monitoring and pervious surface mapping.

Keywords: IKONOS imagery; Urban reflectance; Spectral mixture analysis

1. Introduction

Human settlements occupy a relatively small fraction of Earth's surface area, but their extent, distribution and evolution have enormous impact on environmental and socioeconomic dynamics worldwide. Despite their fundamental importance, urban areas have not been mapped and characterized with remote sensing to the same extent that other land cover types have. Optical sensors on operational satellites provide an efficient means for quantifying past and present distributions of human settlements as well as their physical reflectance properties. This is important at two scales. At a global scale, it is important to understand the physical characteristics that distinguish developed urban areas from other types of human modified and undeveloped land surfaces in order to map and monitor the extent and evolution of urban areas with moderate resolution (20–30 m) optical sensors. The reflectance properties of the urban mosaic are central to both the discrimination of urban land cover and the understanding of its role in the urban environment. At the intraurban scale, it is important to constrain the effect that urban land cover and building materials have on the immediate physical environment. Optical reflectance characteristics have a direct impact on urban microclimate because they modulate the solar energy flux through the built environment. The spatial scale of the reflectance determines the spatial scale of surface temperature variations which, in turn, have a strong influence on heat flux, convection and urban microclimate. Numerical simulation of atmospheric circulation has now advanced to the point where the effects of the built environment on microclimate and air quality can be modeled—given adequate constraints on physical properties like albedo and fractional vegetation. Detailed characterization of urban land cover also has application to pervious surface mapping and urban vegetation monitoring.

Previous urban remote sensing studies have generally focused on identification of specific materials or land cover

* Tel.: +1-845-365-8354; fax: +1-845-365-8179.
E-mail address: small@LDEO.columbia.edu (C. Small).

0034-4257/$ - see front matter © 2003 Published by Elsevier Inc.
doi:10.1016/j.rse.2003.04.008

classes. Ridd (1995) proposed an urban landcover classification scheme based on the distribution of vegetation, impervious surface and soil (the VIS model) but acknowledged the difficulty of distinguishing between soil and impervious surfaces with optical sensors. Subsequent studies (e.g., Flanagan & Civco, 2001; Liu & Lathrop, 2002; Madhavan et al., 2001) have employed a variety of classification methods (Maximum Likelihood, Unsupervised, Decision Tree) with moderate resolution (30 m) imagery, but traditional hard classification algorithms are impeded by the abundance of spectrally mixed pixels. Mixed pixels are problematic for statistical classification methods because most algorithms are based on the assumption of spectral homogeneity at pixel scale within a particular class of land cover. The classification task is often further complicated by inconsistencies between the thematic classes sought and the reflectance properties that can be discriminated with moderate resolution broadband sensors. Urban areas provide examples of spectrally diverse, scale-dependent thematic classes containing large numbers of pixels that are spectrally indistinguishable from other land cover classes. The diversity of land cover types and scales in the urban mosaic therefore results in relatively high rates of misclassification between urban and other land cover classes. Combining spectral, textural and ancillary information can improve classification accuracy (e.g., Stefanov et al., 2001), but a physical characterization of reflectance is still necessary to accommodate the physical processes that influence the upwelling radiance measured by optical sensors. Several recent studies have used physical rather than statistical classifications of urban land cover in individual cities with some degree of success (e.g., Kressler & Steinnocher, 1996, 2000; Phinn et al., 2002; Rashed, Weeks, Stow, & Fugate, 2002; Small, 2001a; Wu and Murray, 2002). High-resolution aerial photographs reduce the abundance of mixed pixels (e.g., Akbari, Rose, & Taha, 1999), but film-based images are less amenable to multispectral image analysis and classification. Hyperspectral imagery can provide sufficient spatial and spectral resolution to map a wide variety of urban surfaces (e.g., Herold, Gardner, Hadley, & Roberts, 2002), but relatively few cities have yet been mapped with imaging spectrometers.

Characterization of urban reflectance is constrained by the spatial resolution of the sensor. The 30-m resolution of the Landsat ETM+ sensor and the 20-m resolution of the Spot HRV sensor are generally not sufficient to discriminate individual features (e.g., buildings, streets, trees) within the urban mosaic. As a result, almost all the urban pixels imaged by these sensors represent a composite radiance field emanating from several distinct features with different reflectances within the sensor's field of view. This spectral heterogeneity at scales comparable to the ground instantaneous field of view (GIFOV) of the sensor results in a preponderance of spectrally mixed pixels. Mixed pixels violate the cardinal assumption of statistical clustering algorithms commonly used to classify land cover types. The increased spatial resolution of IKONOS imagery provides an opportunity to image urban areas at scales sufficient to resolve many (but not all) of the individual features in the urban mosaic. IKONOS' orbital platform also makes it possible to image a wide variety of urban areas worldwide for a self-consistent analysis and comparison of the reflectance properties of urban land cover. A consistent, physically based description of urban reflectance properties could help to advance our understanding and simulation of urban microclimate by providing spatially explicit constraints on albedo, evapotranspiration and spatial distribution of pervious surface. Characterization of urban reflectance at 4 m scale would also provide constraints on the spectral endmembers and mixing processes responsible for the mixed pixels imaged by moderate resolution sensors. If the scale-dependent reflectance properties of urban mixed pixels could be distinguished from the reflectance properties of other types of land cover it would provide a basis for mapping urban areas in moderate resolution imagery collected over the past 30 years.

The objective of this study is to explore a physical characterization of urban reflectance properties in a variety of urban settings. The characterization will incorporate the spatial scale and optical reflectance properties of the variety of land covers contained in the urban mosaics. Spatial autocorrelation is used to quantify the characteristic scale lengths of urban reflectance within and among different cities. Spectral mixture analysis is used to quantify and compare the reflectance properties of these urban areas. Spectral mixture analysis provides a physically based representation of composite radiance measurements that allows surface reflectance to be described as combinations of spectral endmembers. Representing reflectance as continuous gradations within a spectral mixing space provides a more flexible, and accurate, description than that resulting from classification algorithms that assign each pixel membership in one (and only one) of a small number of classes. It is important to distinguish between identification of specific target materials and the physical representation of the radiance image discussed here. Because many different materials can have indistinguishable reflectance signatures as measured by IKONOS, it is not generally possible to identify specific target materials in these unvalidated spectral mixture analyses. The objective here is to determine the consistency of urban reflectances and to assess the feasibility of using spectral mixture analysis to provide a general and widely applicable representation of these reflectances. The key questions addressed by this study are related to the consistency of urban reflectance properties both within and among a variety of urban areas worldwide. This study uses a collection of 14 IKONOS images provided by the NASA Scientific Data Purchase Program. The acquisition parameters for the NASA-funded IKONOS acquisitions are described in greater detail elsewhere in this volume. Throughout the analysis it is assumed that the spatial variations in radiance measured by IKONOS are primarily

a result of spatial variations in surface reflectance and that spatial variations in atmospheric turbidity are not significant at the scale of hundreds of meters or less. Hence radiance will be used when referring to the IKONOS measurements and reflectance will be used when referring to the surfaces from which the radiance emanates.

2. Scales of urban reflectance

The spatial scale of urban reflectance influences physical processes like surface heating and convection as well as the spectral mixing that produces the mixed pixels observed in moderate resolution imagery. It is important to quantify this scale to better understand both of these processes. The degree to which different cities (and areas within cities) exhibit different scales of spatial variability determines the feasibility of a general characterization of urban reflectance. Urban mosaics are composed of a wide variety of features with distinct sizes and reflectance properties, but the size distribution is generally dominated by features at the scale of streets and buildings. The reflectance of an individual feature will generally have some degree of internal variability that is small compared to the reflectance contrast with other features at a scale of 1 to 4 m. This is why individual features like streets and buildings can be usually discriminated in IKONOS imagery. The spatial scale of reflectance variability is therefore determined by the size distribution of individual features in the urban mosaic. In the context of this study, the characteristic scale length refers to the linear dimension of the features of greatest areal abundance. For a typical urban mosaic it is more informative to refer to a range of lengths encompassing the most areally abundant features.

Spatial autocorrelation of IKONOS panchromatic imagery can provide a quantitative measure of the characteristic spatial scales of urban reflectance. The properties of the autocorrelation function as applied to remotely sensed images are described in detail by Getis (1994) and Wulder and Boots (1998). At small lag distances the internal

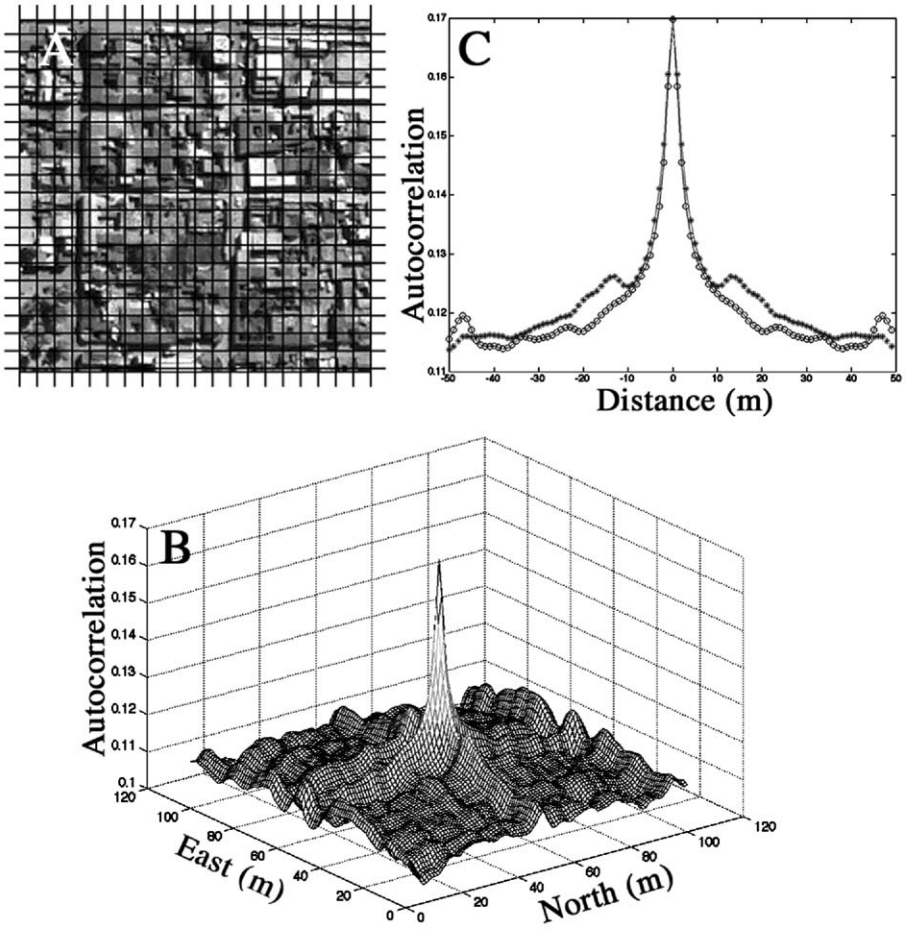

Fig. 1. Characteristic scale length of urban reflectance. IKONOS panchromatic imagery of Caraz Peru (A) shows spatial variations in visible/near infrared (VNIR) radiance resulting from the mosaic of roofs, streets, and open spaces. The superimposed grid spacing is 10 m. (B) The normalized two-dimensional (2D) spatial autocorrelation function (ACF) of a 100 × 100-m subscene shows the azimuth dependence and quasi-periodic structure resulting from the dominant scale of building size and street layout. (C) Asymptotic behavior of orthogonal one-dimensional autocorrelation functions extracted from the 2D ACF shows the consistency of the slope of the central peak. The scale lengths estimated from the 0.1-slope threshold of these two functions are 10 and 12 m and are consistent with the size of most features in (A). Includes materials © Space Imaging.

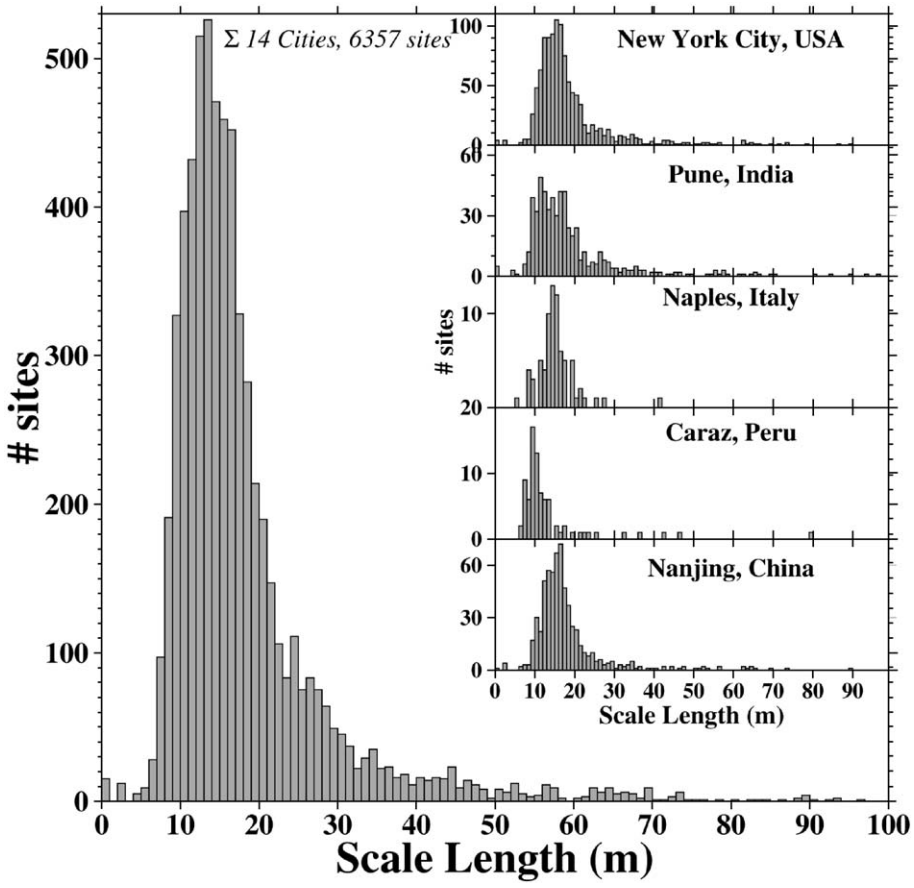

Fig. 2. Distribution of scale lengths for a variety of urban areas. Each of the 6357 sites corresponds to a 100 × 100-m subscene of IKONOS panchromatic imagery. The distribution of scale lengths for the 14 cities indicates that characteristic scales are consistently between 10 and 20 m. Inset histograms show distributions for different cities.

consistency in the reflectance of individual features results in high correlations, but as the lag distance approaches the characteristic spatial scale of the mosaic the reflectance contrast between adjacent features causes the autocorrelation to decrease. The width of the central peak of the autocorrelation therefore provides an indication of the spatial scale of the individual features that contribute significant variance to the observed radiance field. Secondary peaks in the function indicate repetitive patterns in the reflectance at scales and azimuths where bright and dark features are aligned in phase. In this study, two-dimensional (2D) autocorrelation functions (ACFs) are used to estimate the characteristic spatial scale of urban reflectance and to assess the consistency of these scales within and among a variety of urban areas worldwide. For each city, 2D ACFs are calculated for a number of 100 × 100-m subscenes of IKONOS panchromatic imagery, and characteristic scale length estimates are derived from each ACF. The scale length is estimated as the lag distance at which the radial average of the 2D ACF attained a radial slope of 0.1 times the maximum slope of the central peak. The choice of 0.1 is rather ad hoc but the slope of the ACF diminishes asymptotically with distance between the central peak and the first trough so the scale length estimates are not very sensitive to the precise value used for the slope threshold below ~0.1. The slope threshold returned estimates that were consistent with random measurements of feature size from several images. In most of the cities investigated here the 2D ACF indicated the direction and scale of the dominant street grid pattern as radial ridges of higher correlation, but the central peaks are consistently axisymmetric (Fig. 1).

A wide variety of urban areas have similar distributions of scale lengths. Fig. 2 shows scale length distributions for some of the cities investigated and the total distribution of

Fig. 3. False color composites of IKONOS MSI imagery (left) and corresponding principal components (right) for 14 urban areas. Natural color composites of visible bands (R/G/B = 3/2/1) do not discriminate between vegetation and low albedo surfaces as effectively as false color composites (R/G/B = 3/4/1) incorporating the NIR band 4. False color composites of the three low-order principal components (R/G/B = PC1/PC2/PC3) minimize visible band correlations thereby enhancing contrast between surfaces with subtle differences in reflectance. The first principal component corresponds to albedo with bright areas appearing red in all but one image (blue in She Xian). The second principal component corresponds to high NIR reflectance so vegetation appears green. The third principal component is orthogonal to the primary mixing plane so pixels with relatively low proportions of PC1 and PC2 and more pronounced nonlinear mixing outside the primary mixing plane span the range from black to blue. Each image is 1 km^2. Includes materials © Space Imaging.

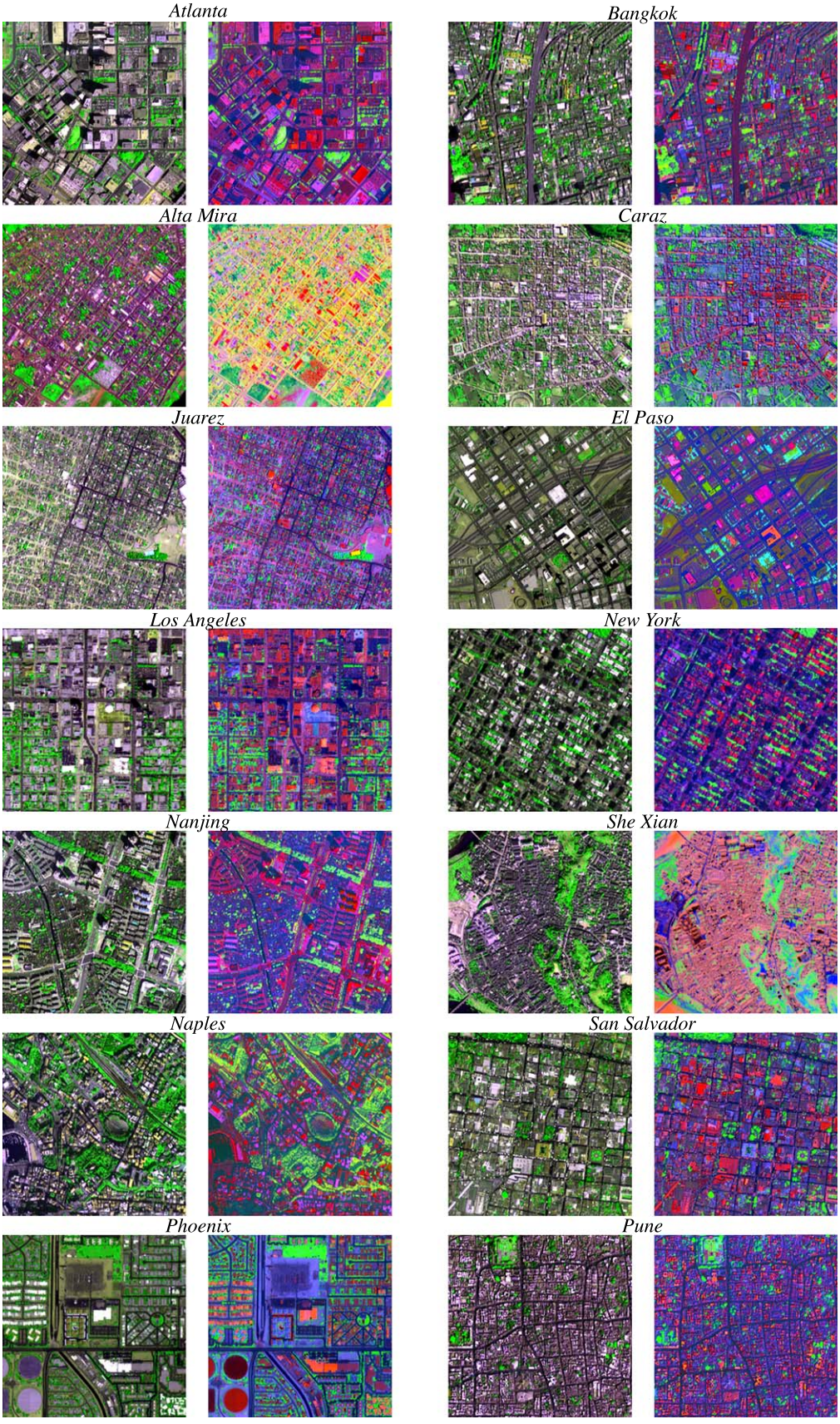
Atlanta
Bangkok
Alta Mira
Caraz
Juarez
El Paso
Los Angeles
New York
Nanjing
She Xian
Naples
San Salvador
Phoenix
Pune

all 14 cities. The total number of 100 × 100-m estimates calculated for each city was determined by the size of the IKONOS image and the total built-up area within each image. All of the large cities had similar skewed distributions like those in Fig. 2. Some of the smaller cities did not provide a large enough number of subscenes to attain a strongly skewed distribution. All the cities investigated, except Alta Mira and She Xian, had similar distributions with modal scale lengths between 10 and 20 m. These smaller cities had smaller scale lengths. These scale length distributions explain why moderate resolution sensors with GIFOVs greater than 10 m rarely resolve individual features in urban areas. This also suggests that a significant percentage of the 4-m IKONOS MSI pixels should image spectrally homogeneous features within urban mosaics with scale lengths greater than 10 m. Urban areas with scale lengths of 10 to 20 m will still have a significant percentage of mixed pixels because the 4-m GIFOV is similar enough to the scale length to result in a significant number of boundary pixels spanning two or more features. The larger the characteristic scale length of features in the urban mosaic, the higher the percentage of spectrally homogeneous pixels and the lower the percentage of mixed pixels. The panchromatic autocorrelation provides a conservative estimate of spectral heterogeneity because spectrally distinct features can have similar VNIR albedos as imaged by IKONOS' panchromatic band.

3. Spectral mixing

Spectral mixture analysis (SMA) provides a systematic way to quantify spectrally heterogeneous urban reflectance. SMA is based on the observation that, in many situations, radiances from surfaces with different "endmember" reflectances mix linearly within the IFOV (Nash & Conel, 1974; Singer, 1981; Johnson, Smith, Taylor-George, & Adams, 1983; Singer & McCord, 1979). This observation has made possible the development of a systematic methodology for SMA (Adams et al., 1986, 1989, 1993; Gillespie et al., 1990; Smith, Ustin, Adams, & Gillespie, 1990; Roberts, Smith, & Adams, 1993) that has proven successful for a variety of quantitative applications with multispectral imagery (e.g., Adams et al., 1995; Elmore, Mustard, Manning, & Lobell, 2000; Pech, Davies, Lamacraft, & Graetz, 1986; Roberts, Batista, Pereira, Waller, & Nelson, 1998; Smith et al., 1990). If a limited number of distinct spectral endmembers are known, it is possible to define a "mixing space" within which mixed pixels can be described as linear mixtures of the endmembers. Given sufficient spectral resolution, a system of linear mixing equations may be defined and the best fitting combination of endmember fractions can be estimated for the observed reflectance spectra. The strength of the SMA approach lies in the fact that it explicitly takes into account the physical processes responsible for the observed radiances and therefore accommodates the existence of mixed pixels.

The diversity of land covers in the urban mosaic influences the topology of the mixing space while the spectral dimensionality of the image is constrained by the number of bands and their spectral resolution. The limited spatial and spectral resolution of the IKONOS sensor results in a projection of a high-dimensional mixing space onto a lower-dimensional representation that is constrained by the ability of the sensor to discriminate different surface reflectances at GIFOV scales. Analyses of AVIRIS hyperspectral imagery suggest that some urban areas have as many as 30 to 50 spectral dimensions (Green & Boardman, 2000; Small, 2001c), but the IKONOS sensor can resolve only four of these dimensions at most. A central question of this analysis is whether these four dimensions provide an adequate basis for a systematic characterization of urban reflectance. Is the information content provided by the IKONOS sensor sufficient to characterize the differences in scale and reflectance between urban areas and other land cover types in a consistent manner?

In this study, the mixing space characterization is provided by a principal component transformation of the multispectral imagery. The principal component rotation minimizes the correlations among bands and enhances the contrast between different surface reflectances. The accompanying eigenvalue distribution provides a quantitative estimate of the variance partition between the signal- and noise-dominated principal components of the image. With hyperspectral sensors this partition and the number of signal-dominated components can form the basis of a dimensionality estimate of the image (Green & Boardman, 2000). With broadband sensors like IKONOS, the four-band limit to the number of distinguishable dimensions is generally less than the number of spectrally distinct endmembers (and hence the inherent dimensionality). The multidimensional feature space of the low-order principal components represents the spectral mixing space that can be used to define spectral mixtures as combinations of spectral endmembers (Boardman, 1993;

Fig. 4. Mixing space representation of IKONOS MSI imagery. Normalized eigenvalues (left column) give the variance partition among the principal components. The two-dimensional scatterplots of the principal components are projections of the three low-order dimensions of a four-dimensional spectral mixing space. The side view shows the two dimensions associated with the majority (>96%) of the variance while the top and end views incorporate the third dimension. Variance in the third dimension is primarily associated with nonlinear mixing along the "gray axis" between the high and low albedo endmembers and generally accounts for less than 3% of the total variance. The fourth dimension (not shown) contributes less than 1% of the variance but still contains coherent spectral information. Orthogonal projections of spectral mixing spaces in a variety of urban areas show a similar structure with a narrow triangular mixing space spanned by high albedo (H), low albedo (L) and vegetation (V) endmembers. Straight edges correspond to linear mixing among endmembers while convex edges indicate nonlinear mixing. Tapering of the mixing space approaching the Vegetation endmember suggests that a three-component mixing model is very well constrained for vegetation fractions. The apex seen in the third dimension generally corresponds to a soil (S) endmember.

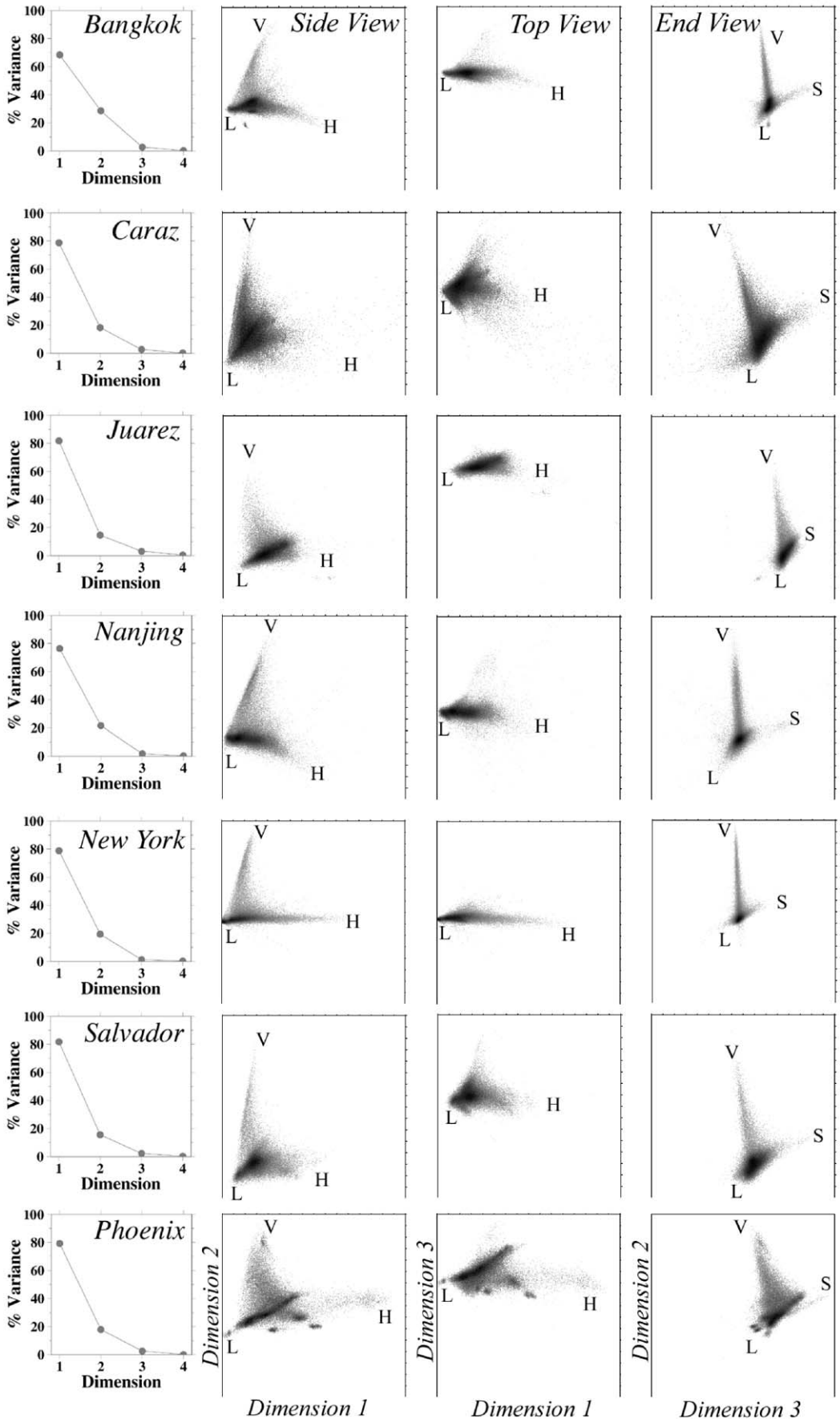
Bangkok
Caraz
Juarez
Nanjing
New York
Salvador
Phoenix
% Variance
Dimension
Side View
Top View
End View
V
L
H
S
Dimension 2
Dimension 1
Dimension 3

Jackson, 1983; Johnson, Smith, & Adams, 1985). The mixing space could be represented with scatter plots of the unrotated bands but using scatter plots of the principal components (PCs) provides an ''optimal'' projection of the mixing space because the PC rotation orders the projections with respect to the variance they contribute to the scene.

In this analysis, a minimum noise fraction (MNF) principal component transformation is used to project the mixing space onto a series of 2D scatter plots. These scatter plots are referred to geometrically with the ''side view'' corresponding to the projection of the two lowest order PCs containing the largest amount of image variance. The ''end view'' and ''top view'' incorporate the third dimension of the mixing space and help to represent the cloud of pixels occupying the three low-order dimensions of the mixing space as a 3D object. The MNF transformation implemented in ENVI is analogous to the maximum noise transformation described by Green, Berman, Switzer, and Craig (1988) but differs in the ordering of the principal components from high to low signal variance (RSI, 2000). With IKONOS imagery, the MNF transformation usually produces principal components similar to those resulting from a traditional covariance-based PC rotation but offers the added benefit of normalizing the eigenvalues relative to the variance of the sensor noise estimate. For this analysis, all MNF transformations were applied using noise covariance statistics derived from a July 2001 acquisition over the Central Park Reservoir in New York City under relatively clear atmospheric conditions. The Reservoir is an enclosed, noncirculating body of water ~600 m in diameter with negligible reflectance from suspended sediment or biological productivity and therefore provides a reasonable approximation of a ''dark target''. Normalized eigenvalue distributions quantify the partition of variance among the principal components indicating how many spectral dimensions are required to represent the information content in the image. The larger eigenvalues are associated with the low-order principal components representing the dominant reflectance patterns while the smaller eigenvalues are associated with the higher-order principal components associated with the pixel scale variance commonly assumed to be noise. The signal-to-noise ratio of the IKONOS sensor is sufficiently high that all of the principal components in all scenes investigated showed significant information content well above the noise level. The eigenvalue distributions of IKONOS imagery therefore do not indicate the dimensionality of the image but rather the variance partition among the dimensions.

Subscenes of the 14 images used in this analysis are shown in Fig. 3. The full-size images vary in area, cloud cover and location, so 1-km^2 subscenes are used for most of the comparative analyses. These subscenes were chosen to represent the spectral diversity typically observed within the built-up core of each city. The results are generally consistent with those of the larger subscenes but are more easily compared because of their uniform size. The false color composites incorporating the NIR band (R/G/B = 3/4/1) emphasize the distinction between vegetation and low albedo surfaces. False color composites of the three low-order principal components maximize the spectral contrast between objects of different reflectance, but they also reveal a consistency in the reflectance of the urban areas used in this study. In each case, the low-order principal component (PC1) corresponds to the overall albedo of the image. Hence, bright features usually appear red in Fig. 3. The second principal component distinguishes vegetation from nonvegetated surfaces resulting in a correspondence of the green areas in the composites in Fig. 3. The third principal component accounts for only a few percent of the total image variance so areas that appear blue are characterized by lower albedo unvegetated areas with other types of reflectance such as dark soils.

Spectral mixing spaces provide a self-consistent basis for comparison of urban reflectance characteristics (Small, 2002a). IKONOS MSI imagery shows a simple, but consistent, spectral mixing space structure for the urban areas investigated in this study. The similarity of the triangular mixing spaces shown in Fig. 4, as well as those not shown, indicates that all 14 of the urban areas in this study have a consistent mixing space topology in the form of a narrow triangular cloud of pixels. The distribution is referred to as narrow because the variance of the two primary dimensions is considerably greater than the other dimensions. Each principal component is scaled by its full range of values so the relative widths of the mixing space are exaggerated. The actual variance is indicated by the corresponding eigenvalue so the third and fourth dimensions are much ''thinner'' than the first two dimensions. In each case, the three endmembers defining the apexes of the triangular mixing space correspond to high albedo (H), low albedo (L) and vegetation (V) reflectances. Although the internal distributions of mixed pixels within the mixing spaces vary, the overall form is consistent. The apexes of the primary 2D mixing space corresponding to the spectral endmembers are generally well defined and the edges between the apexes are generally straight or concave. This indicates that the mixing among

Fig. 5. Mixing spaces for nonurban land cover. At 1 km^2 scales, other types of land cover do not generally produce the triangular mixing space characteristic of urban land cover. While these mixing spaces do show cases of linear mixing among well-defined endmembers, nonlinear mixing is evident from the convex edges of the mixing spaces. Multiple scattering within the open canopy vegetation of the Argentinian pampa produces strong nonlinear mixing. The mixing space representing the sparsely vegetated Peruvian highland has a well-defined low albedo endmember, but mixing becomes increasingly nonlinear as albedo increases along dimension 1. The densely vegetated mountains in central China produce a mixing space dominated by illumination differences in which an exposed soil endmember resides at the bottom of the secondary dimension. The spectrally diverse riparian land cover of the Brazillian Amazon most closely resembles the triangular mixing space seen in urban areas. Its primary mixing space is dominated by two linear mixing continua and complex topology at the high albedo apex.

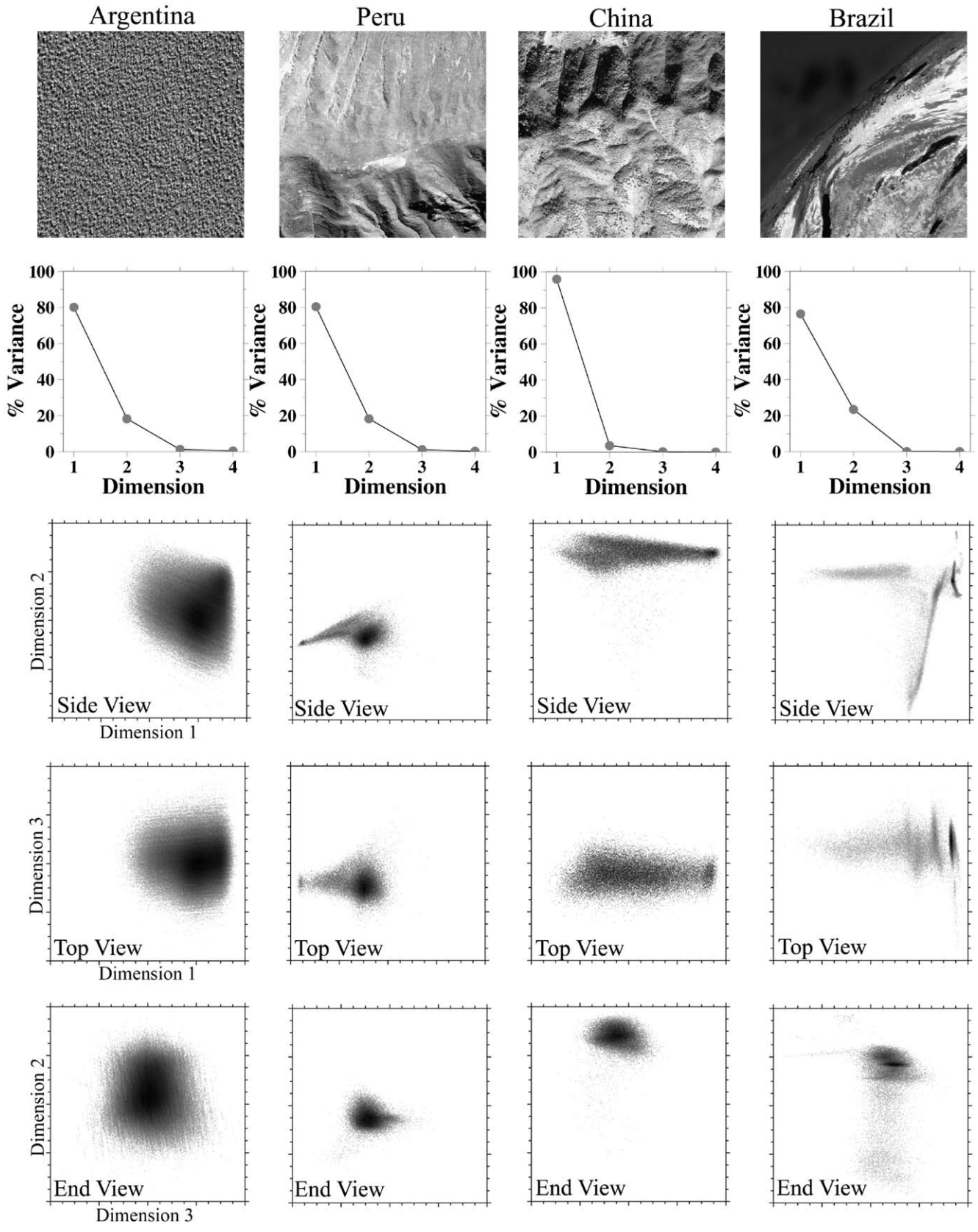
Argentina
Peru
China
Brazil
% Variance
Dimension
Dimension 2
Dimension 1
Dimension 3
Side View
Top View
End View

these three endmembers is primarily linear, while nonlinear mixing is indicated by the convex edges seen in the third dimension. The lower variance of the third dimension indicates that the magnitude of the nonlinear mixing is small compared to the linear mixing represented in the two primary dimensions. This suggests that a three-component linear mixing model may provide a consistent and accurate way to represent urban reflectances. A more detailed discussion of the mixing space concept is provided by Boardman (1989a,b).

In contrast to the consistency in urban mixing spaces, the land cover mosaics in nonurban environments produce a diversity of mixing space topologies. Fig. 5 shows examples of four IKONOS images selected from different environments and their mixing space representations. Even though all of these environments contain several different types of land cover of varying reflectance, none of their mixing spaces resembles the triangular mixing space that is characteristic of the urban areas used in this study. Agricultural areas do, however, often exhibit a triangular mixing space similar to those of the urban areas. These triangular mixing spaces bear a strong resemblance to the "tasseled cap" feature space described by Kauth and Thomas (1976) and can be considered representative of visible/near infrared reflectance in certain instances where the scene contains high albedo, low albedo and vegetation endmembers simultaneously. In fact, it would be possible to define a transformation for IKONOS imagery analogous to the tasseled cap transform defined for Landsat TM and MSS. The spectral mixture analysis described below is, however, preferable to a predefined transformation because it can represent a wider variety of spectral endmembers and can accommodate different atmospheric effects.

The topology of the mixing spaces depends on the combination of reflectance patterns contained within the image. In general, the larger urban images used in this study had mixing spaces similar to those of the 1-km images shown in Fig. 4. Other 1-km images chosen from areas surrounding the built-up part of each city sometimes had different mixing space topologies, but inclusion of the built-up areas generally results in the triangular topology seen in Fig. 4. A similar topology is seen in the low-order dimensions of urban mixing spaces generated from Landsat and AVIRIS imagery (Small, 2001b). Spectral dimensionality does, however, tend to diminish at smaller spatial scales (Small, 2001c). In the case of IKONOS urban imagery, this generally results in a different partition of variance among the principal components rather than a change in mixing space topology. Fig. 6 indicates that the larger urban scenes generally have a greater fraction of the variance in the second principal component as a result of a greater percentage of vegetated area. The 1-km images generally have a greater fraction of variance associated with the low-order dimension. This is not surprising as the smaller areas have a lower areal percentage of vegetation and are dominated by spectral variations along the "gray axis" between the high albedo and low albedo endmembers.

The topologic consistency of the mixing spaces is complemented by a consistency in endmember reflectances. Fig. 7 shows the radiance vectors corresponding to pixels at the apexes of each mixing space. The amplitudes of the endmembers are variable but the shape is remarkably consistent. The low albedo endmember generally corresponds to deep shadow so its shape represents the atmospheric path radiance component that is present in every pixel. The most pronounced differences are related to atmospheric conditions, but there is also a moderate correlation (0.67) between the peak amplitude of the high albedo endmember and the solar zenith angle at the times the images were acquired. The collection geometry varied between elevation angles of 61° and 87°. Given the

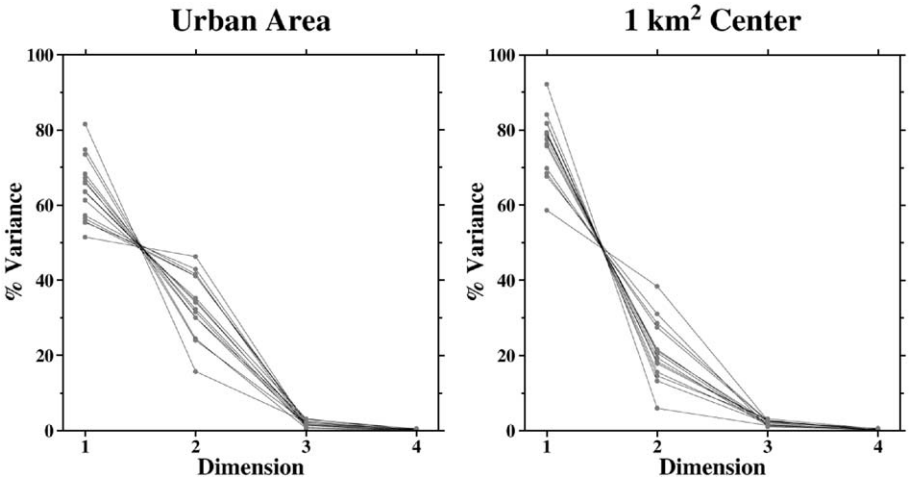

Fig. 6. Scale dependence of variance partition. Normalized eigenvalue distributions for larger urban areas (left) indicate that the second dimension of the mixing space accounts for much of the variance (20–50%) in urban reflectance at spatial scales of several kilometers. Eigenvalue distributions of smaller (1 km^2) city center areas show a greater fraction of variance associated with the primary dimension spanned by high and low albedo endmembers. The difference is due to the greater abundance of vegetated area within the larger images than within the 1-km^2 city centers.

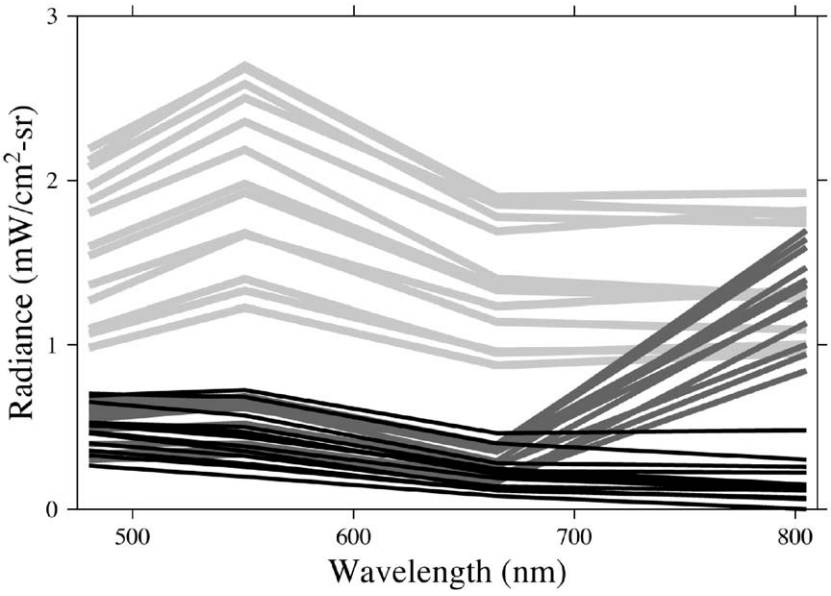

Fig. 7. Spectral endmembers. Radiance vectors corresponding to the apexes of the triangular mixing spaces show a remarkable consistency of form, although amplitude is variable. Variations in amplitude result from actual differences in endmember reflectance as well as differences in illumination and atmospheric conditions. The slope of the low albedo endmembers (thin curves) is consistent with wavelength-dependent atmospheric scattering effects. IKONOS DNs were converted to radiance using the calibration coefficients provided by Space Imaging and NASA (Zanoni et al, Pagnutti et al, this volume).

differences in solar zenith, collection geometry, atmospheric turbidity, it is surprising that the amplitude differences among the endmembers are not greater.

4. Linear mixture modeling

The consistency of the spectral mixing space for a variety of urban areas suggests that a simple three-component linear mixture model may provide a consistent, general characterization of urban reflectance. Representing urban reflectance, of individual pixels or aggregate distributions, as three-component mixtures makes it possible to compare reflectance patterns within and among cities. The high albedo, low albedo and vegetation endmembers also provide a useful physical description since albedo and vegetation cover are two of the primary surface properties that control urban microclimate. While the statistical moments of the mixing space (mean, variance, skewness, etc.) provide a description of the aggregate reflectance of an urban area, each individual pixel within the aggregate can be described by its relative areal abundance of each endmember. Spectral mixture modeling provides a way to derive estimates of endmember abundance for individual pixels.

Inversion of the urban three-component linear mixing model for each pixel yields fraction estimates for each endmember. The linear three-component mixing model is given in continuous form by:

$$\mathbf{R}(\lambda) = f_{\mathrm{H}}\mathbf{E}_{\mathrm{H}}(\lambda) + f_{\mathrm{V}}\mathbf{E}_{\mathrm{V}}(\lambda) + f_{\mathrm{L}}\mathbf{E}_{\mathrm{L}}(\lambda) \quad (1)$$

where $\mathbf{R}(\lambda)$ is the observed radiance profile, a continuous function of wavelength λ. The $\mathbf{E}(\lambda)$ are the spectra corresponding to the high albedo (H), vegetation (V) and low albedo (L) endmembers. The corresponding endmember fraction estimates we seek are f_{H}, f_{V} and f_{L}. The discrete implementation of the model, applicable to IKONOS MSI radiances, is given by:

$$\begin{aligned} f_{\mathrm{H}}\mathbf{e}_{11} + f_{\mathrm{V}}\mathbf{e}_{12} + f_{\mathrm{L}}\mathbf{e}_{13} &= \mathbf{r}_1 \\ f_{\mathrm{H}}\mathbf{e}_{21} + f_{\mathrm{V}}\mathbf{e}_{22} + f_{\mathrm{L}}\mathbf{e}_{23} &= \mathbf{r}_2 \\ f_{\mathrm{H}}\mathbf{e}_{31} + f_{\mathrm{V}}\mathbf{e}_{32} + f_{\mathrm{L}}\mathbf{e}_{33} &= \mathbf{r}_3 \\ f_{\mathrm{H}}\mathbf{e}_{41} + f_{\mathrm{V}}\mathbf{e}_{42} + f_{\mathrm{L}}\mathbf{e}_{43} &= \mathbf{r}_4 \end{aligned} \quad (2)$$

where $\mathbf{r}_{\mathrm{i}}$ is the observed radiance vector corresponding to discrete estimates of integrated radiance within the four IKONOS MSI bands. The $\mathbf{e}_{ij}$ are the endmember radiance vectors corresponding to the high albedo (H), vegetation (V) and low albedo (L) endmembers. The indices i and j indicate the spectral band and endmember of each element, respectively. An additional unity sum constraint equation can be incorporated to urge the fractions to sum to 1. With four or less endmembers, the system has more equations than unknowns and can be solved for an "optimal" set of endmember estimates chosen to minimize misfit to the observed radiance vector.

The overdetermined linear mixing model, incorporating measurement error, can be written in matrix notation as:

$$\mathbf{r} = \mathbf{E}\mathbf{f} + \varepsilon \quad (3)$$

where ε is an error vector which must be minimized to find the fraction vector $\mathbf{f}$ which gives the best fit to the observed radiance vector $\mathbf{r}$. There are a number of ways to solve this type of problem (e.g., Pech et al., 1986; Settle & Drake,

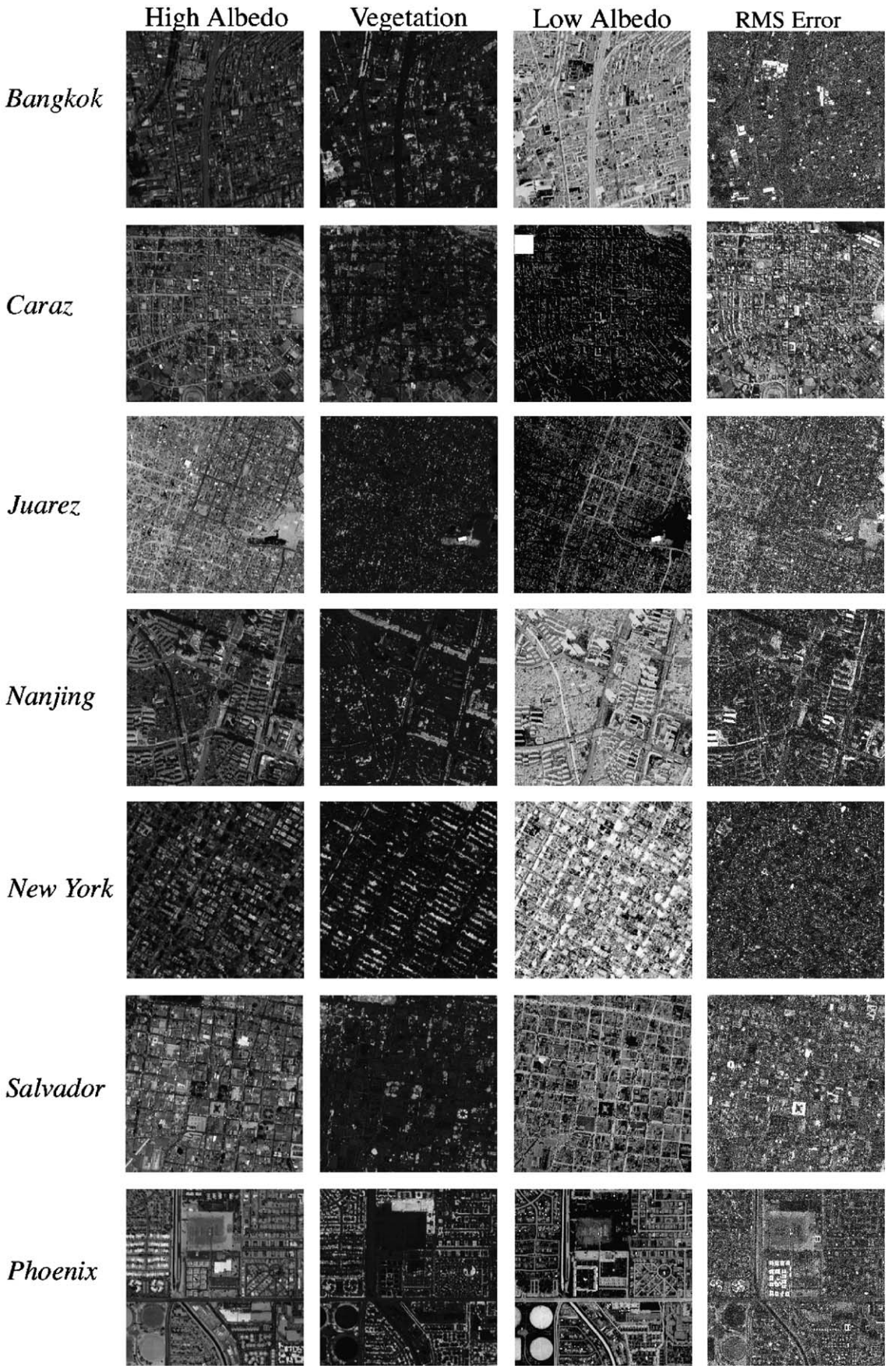
High Albedo
Vegetation
Low Albedo
RMS Error
Bangkok
Caraz
Juarez
Nanjing
New York
Salvador
Phoenix

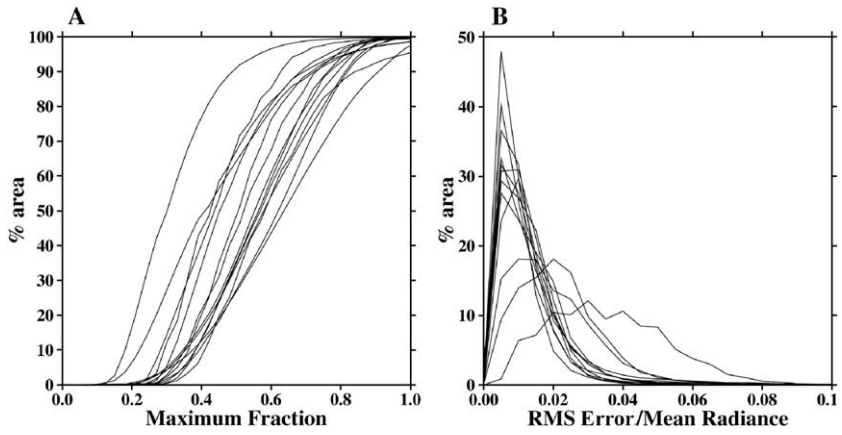

Fig. 9. Maximum endmember fractions and RMS error distributions. (A) The cumulative distributions of the largest endmember fraction of each pixel span the full range of permissible maximum fractions. Cities with significant areas of unmodeled soil (Caraz, Juarez, Phoenix, Pune, and Salvador) have more than 10% area with maximum fractions less than 0.33. The three-component model does not account for the soil endmember and cannot replicate the spectra of these pixels. (B) The RMS of the differences between the modeled and observed radiance vectors is normalized by mean pixel radiance to account for the magnitude of the misfit relative to the amplitude of the observed radiance vector. Distributions of radiance-normalized RMS error are consistently low with error amplitudes less than 3% of the mean radiance of the corresponding pixel. The three urban areas with higher errors (Bangkok, Caraz, Salvador) correspond to examples with an unmodeled fourth endmember in the third dimension.

1993; Smith, Johnson, & Adams, 1985; Smith et al., 1990). The procedure used to invert the urban three-component linear mixing model for endmember reflectances is described in detail and the stability of the inversion is demonstrated in Small (2001a). A unit sum constrained least squares inversion of the three-component model was performed on all 14 of the 1-km images. The endmember fraction images for seven of the 1-km IKONOS images are shown in Fig. 8. Most of the urban areas used in this study were characterized by high fractions of the low albedo endmember. This represents the abundance of shadow as well as the frequent use of low albedo building materials in urban areas. Shadow can mask true target reflectance thereby increasing the apparent abundance of low albedo targets.

Inversion of the linear mixing model produces areal abundance estimates, but these should not be interpreted in the context of ‘‘subpixel resolution’’. Areal estimation of an individual feature within a single pixel is complicated by the spatial variation in the sensor’s response function. The nonlinear mixing effects of the sensor’s point spread function can introduce significant error when the spatial scale of the endmember fractions is comparable to the scale of the GIFOV. The endmember fraction estimates are most accurate when the spatial scale of the endmember components is small relative to the GIFOV. This nonlinear mixing is further complicated by the application of modulation transfer function compensation (MTFC) filters. The MTFC procedure attempts to compensate for the spatial averaging effects of the point spread function by increasing the contrast of adjacent pixels (Pagnutti, Ryan, Kelly, & Holekamp, this issue; Ryan et al, this issue; Zanoni et al., this issue). To quantify the effect (positive or negative) of the MTFC on the fraction estimates, it would be necessary to compare field validation measurements with estimates derived from the same imagery with and without MTFC applied. All but two of the IKONOS images (New York and Hollywood) used in this study had MTFC applied as they were acquired before the NASA investigators were given the option of processing without MTFC.

Cumulative distributions of the maximum fractions for each pixel in each image are shown in Fig. 9A. These distributions indicate that most of images have fraction distributions spanning the full range (0.33 to 1.0) of allowable abundances. Maximum fractions near 1.0 are associated with pure pixels while maximum fractions near 0.33 are associated with mixed pixels. Maximum fractions below 0.33 indicate that the three-endmember model did not accurately represent some of the radiance vectors. In this study, cities with large areas of unmodeled soil had significant numbers of pixels with fractions that did not sum to unity. For some of these cities (Caraz, Juarez, Phoenix, Pune, Salvador), a four-endmember model containing a soil endmember would have been more appropriate.

Several of the urban areas in this study had mixing spaces that could accommodate a fourth endmember. In most of these cases, this fourth endmember would corre-

Fig. 8. Endmember fraction estimates and linear mixing model errors. Inversion of a constrained, three-component linear mixture model results in three endmember fraction estimates for each pixel in the image. Endmember fraction images range from 0 (black) to 1 (white). The RMS error for each pixel is calculated for the difference between the observed radiance and the forward implementation of the linear model using the endmember vectors and the endmember fraction estimates. RMS error images range from 0% to 6% and are displayed with a 2% linear stretch to emphasize specific features not well fit by the three-component linear model. Most urban areas have a strong low albedo component corresponding to shadow and the low surface reflectance of many building materials.

spond to soil, but in some of the urban areas the fourth endmember appears to represent a spectrally distinct high albedo roofing material. Adding a fourth endmember will generally reduce the RMS error so the three-component linear mixing model provides a conservative indication of how well linear mixture models can be expected to represent urban reflectance in IKONOS imagery.

The suitability of the linear mixing model is indicated by the magnitude and distribution of the RMS error—the root mean square of the difference between the observed radiance vectors and the modeled radiance vectors. The modeled radiance vector is generated by forward implementation of the linear mixing model as a fraction-weighted sum of the endmember radiance vectors using the estimated fractions. Distributions of normalized errors are shown in Fig. 9B. The RMS error of each pixel is normalized by the mean radiance of the pixel to indicate the magnitude of the error relative to the amplitude of the observed radiance vector. Fig. 9B indicates that the majority of the pixels were fit to within 3% of the amplitude of the observed radiance vector in most scenes. Three of the images used in the study had larger errors. These images had mixing spaces indicating the presence of a fourth endmember. It is encouraging, however, that even in these cases the errors rarely exceed 6% of the observed amplitude.

A low RMS error is necessary but not sufficient condition for accurate estimation of actual areal abundances of specific endmember materials within the GIFOV. In other words, a small error does not guarantee that the endmember abundances will agree with field validation measurements, but a large error does indicate that the endmembers and fraction estimates do not accurately represent the composite radiance measured by the sensor for a given pixel. Field validation is necessary if the endmember abundances are to be related to specific quantities of endmember materials on the ground. The fraction estimates produced in this study have not been validated with field measurements, but the small errors to the observed radiances indicate that the three-component linear model is generally well posed and worthy of validation and further investigation.

It is important to distinguish between spectral endmember abundances and specific target materials. Hyperspectral imagery of urban areas reveals the presence of as many as 60 spectral dimensions (Green & Boardman, 2000; Small, 2001c) related to the wide variety of spectrally distinct building materials (Herold et al., 2002). Many of these materials are spectrally indistinguishable with broadband sensors like IKONOS. High albedo roofing material is often indistinguishable from high albedo soil while many low albedo materials are indistinguishable from clear water and deep shadow. Broadband sensors may not be able to discriminate spectrally similar materials but the continuum representation provided by mixture models accommodates a far wider range of targets and conditions than hard classification because it represents the continuous gradations among spectrally distinct materials.

5. Potential applications

Representation of multispectral radiances, or surface reflectances, as spectral endmember abundances provides a simple way to describe reflectance properties imaged by the IKONOS sensor. The strength of the spectral mixture model is its ability to represent a wide variety of surface reflectance types as simple combinations of endmember abundances. The inversion of the linear mixing model is computationally trivial compared to statistical classifications like maximum likelihood. Spectral mixture analysis is preferable to ‘‘hard classification’’ for many physical science applications because it accommodates the fundamental physical process responsible for the preponderance of mixed pixels observed in almost all multispectral imagery. Representing a high-dimensional urban mixing space with only three endmembers is obviously a gross simplification, but it does provide a more flexible representation than hard classifications which attempt to represent a continuum of reflectance characteristics with exclusive membership in one of a limited number of idealized classes. Endmember fraction distributions can also be ‘‘hardened’’ into a finite number of thematic classes if necessary (Adams et al., 1995; Roberts et al., 1998). Spectral mixture models have the added advantage of producing output in physically intuitive units (fractional area). Relative abundances of high and low albedo surface and vegetation can be converted to physical quantities like albedo, pervious surface area and leaf area index more easily than radiance measurements can and more accurately than thematic classes can.

Vegetation fraction estimates derived from IKONOS imagery provide a tool to monitor urban vegetation health and abundance. An example of intraurban variations in vegetation fraction is shown for Chicago in Fig. 10. The spatial distribution and abundance of vegetation has a direct impact on the urban environment by modulating solar energy flux and evapotranspiration. Urban vegetation may also have an impact on urban air quality as leaves sequester surface reactant pollutants and particulates (Abdollahi & Ning, 2000). Mapping spatial distribution and abundance of urban vegetation is therefore important for modeling urban air quality. IKONOS’ 4-m GIFOV approaches the scale of crown diameter for many tree species. Quantitative assessment of vegetation fraction at this scale could be useful for monitoring defoliation and blight in large urban parks. Vegetation distribution can also be used as a proxy for pervious surface when modeling urban hydrology (Small, 2002b).

Examination of spectral mixing spaces may also prove useful for feature extraction tasks. In spite of its limited spectral resolution, IKONOS’ 11-bit radiometry is capable of distinguishing subtle differences in surface reflectance that would be indistinguishable with 8-bit imagery. IKONOS combination of high spatial resolution and bit depth results in greater clustering within the mixing space. The Phoenix mixing space shown in Fig. 4 provides an example

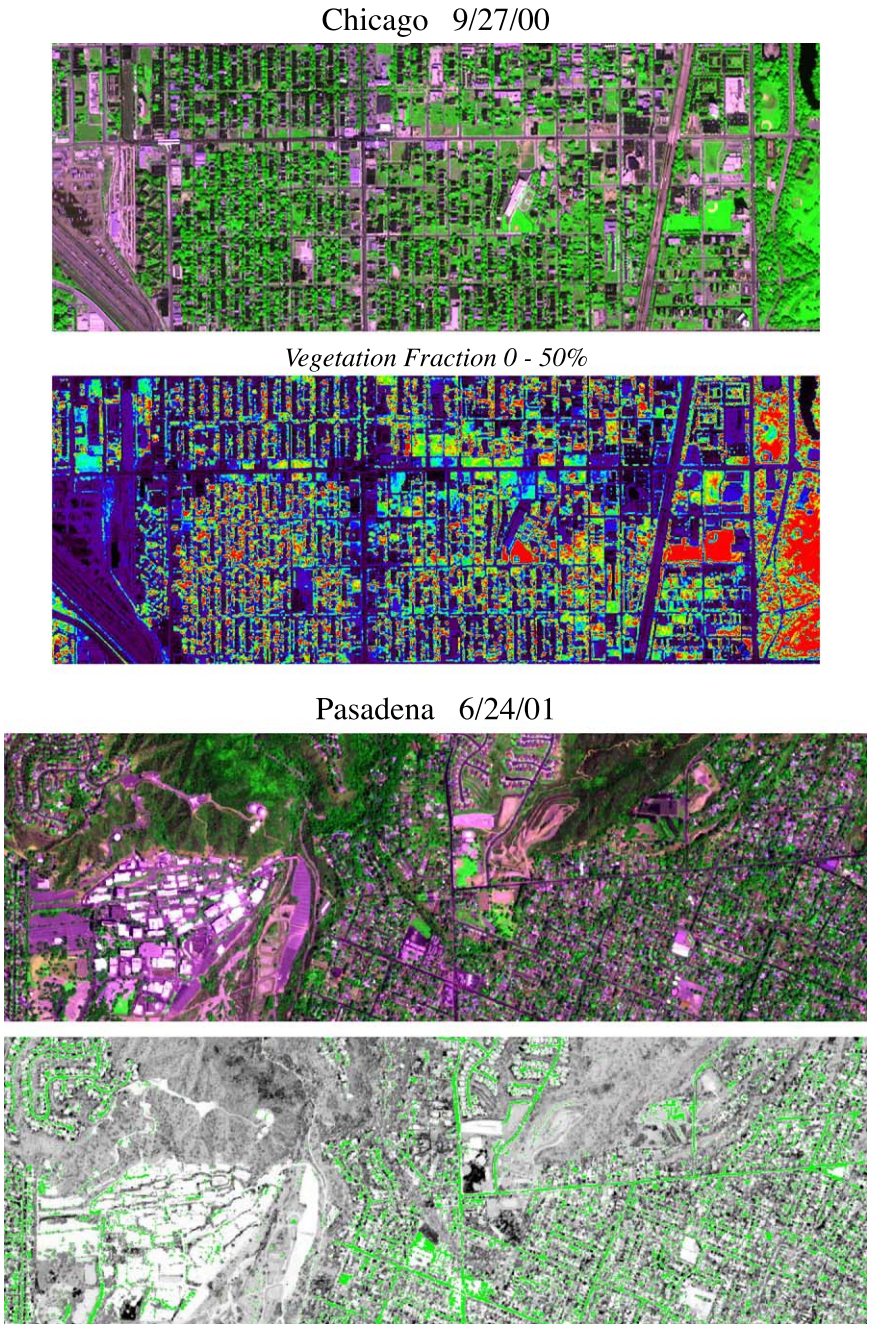

Fig. 10. Example applications of spectral mixture analysis of urban IKONOS imagery. Vegetation fraction estimates have sufficient spatial resolution to map intraurban vegetation abundance at street scale in Chicago. Warmer colors show higher vegetation abundance with fractions greater than 50% saturated red. Localization of features with consistent reflectance properties within the mixing space can facilitate extraction of features like road networks (green) in Pasadena. Includes materials © Space Imaging.

of this clustering (Fig. 4). Targets with distinct and consistent reflectance will appear as distinct clusters in IKONOS' mixing space whereas their reflectance would be mixed with, or indistinguishable from, adjacent features in the mixing space of a sensor with lower spatial resolution or fewer resolvable brightness levels. An example of a fine scale feature extraction from mixing space clustering is shown in Fig. 10. The paved road surfaces in this image of Pasadena have sufficiently consistent and distinct reflectance that they can be discriminated from other low albedo features with relatively high accuracy.

6. Conclusions

Spectral mixture analysis provides a physically based approach to quantify the optical reflectance properties of the urban mosaic. The spectral mixing space concept accom-

modates the inevitable existence of mixed pixels and provides insight into the variety of distinct and gradational reflectance patterns present in IKONOS imagery. The mixing space representation also reveals the presence of spectral endmembers and the extent to which mixing among the endmembers is linear. When mixing is predominantly linear, it is possible to define linear mixture models that can be inverted to yield endmember fraction estimates and measures of misfit to observed data.

Spatial autocorrelation of IKONOS panchromatic imagery provides statistical estimates of the spatial scale of urban reflectance variations. Two-dimensional autocorrelation functions consistently show a well-defined, axisymmetric peak with a width corresponding to the spatial scale of the most areally abundant features. The width of the peak therefore provides an estimate of the characteristic spatial scale of the high contrast reflectance patterns corresponding to individual features within the urban mosaic (roads, buildings, trees, etc.). The distribution of length scale estimates from 6357 sites in 14 urban areas indicates that the majority of sites have characteristic length scales between 10 and 20 m. This explains why urban areas are characterized by spectral heterogeneity when imaged by moderate resolution (20–30 m) sensors. This also suggests that a significant fraction of IKONOS' 4-m pixels will be spectrally heterogeneous in urban imagery. This is supported by the maximum fraction distributions in Fig. 9.

Principal component transformation of urban IKONOS imagery allows reflectance patterns to be interpreted in the context of a spectral mixing space. Eigenvalue distributions of the imagery used in this study indicate that the majority (55% to 95%) of image variance corresponds to albedo variations represented in the first principal component (PC). A significant, but lesser, fraction of image variance is associated with vegetation. In the urban areas investigated here, almost all (>96%) image variance is associated with the first two PCs. The remaining two PCs contain useful information about distinct reflectances not discriminated in the first two PCs and may be useful for isolating additional endmembers. The spectral mixing space defined by the first three principal components consistently takes the form of a triangular scatterplot with linear or concave edges indicating that mixing is predominantly linear. The spectral endmembers residing at the apexes of the mixing space correspond to high albedo, low albedo and vegetation endmembers. The mixing spaces of some of the urban areas used in this study also revealed the presence of a fourth endmember, usually corresponding to soil.

Inversion of a simple three-component linear mixture model produces stable, consistent estimates of endmember abundance fractions for each pixel in the image. RMS misfits between observed radiance vectors and modeled radiance vectors based on fraction estimates are generally less than 3% of the mean of the observed radiance vector. Most of the urban areas used in this investigation are dominated by the low albedo endmember as a result of shadowing and low reflectance building materials. Abundance of vegetation and high albedo features varies considerably within and among cities. Endmember abundance maps derived from IKONOS can be used to constrain spatial variations in solar energy flux and evapotranspiration as well as to map spatial distributions of vegetation and pervious surfaces.

Acknowledgements

The IKONOS data used in this study were provided by Space Imaging through the NASA Scientific Data Purchase program. Includes materials © Space Imaging. This research would not have been possible without the support of the Columbia Earth Institute, CIESIN and the NASA Socio-Economic Data and Applications Center (SEDAC).

References

Abdollahi, K. K., & Ning, Z. H. (2000). Urban vegetation and their relative ability in intercepting particle pollution (PM2.5). *Third Symposium on the Urban Environment, Davis, CA, 1.15*.

Adams, J. B. (1986). Spectral mixture modeling: A new analysis of rock and soil types at the Viking Lander 1 site. *Journal of Geophysical Research*, *91*, 8089–8122.

Adams, J. B., Sabol, D. E., Kapos, V., Filho, R. A., Roberts, D. A., Smith, M. O., & Gillespie, A. R. (1995). Classification of multispectral images based on fractions of endmembers: Application to land cover change in the Brazilian Amazon. *Remote Sensing of Environment*, *52*, 137–154.

Adams, J. B., Smith, M. O., & Gillespie, A. R. (1993). Imaging spectroscopy: Interpretation based on spectral mixture analysis. In C. M. Englert, & P. Englert (Eds.), *Remote Geochemical Analysis: Elemental and Mineralogical Composition* (pp. 145–166). New York: Cambridge Univ. Press.

Akbari, H., Rose, L. R., & Taha, H. (1999). Characterizing the Fabric of the Urban Environment: A Case Study of Sacramento, CA. Report No. LBNL-44688, Lawrence Berkeley National Laboratory, Berkeley, CA.

Boardman, J. W. (1993a). Automating spectral unmixing of AVIRIS data using convex geometry concepts. *Proceedings Third JPL Airborne Earth Science Workshop, Pasadena, CA*.

Boardman, J. W. (1989b). Inversion of imaging spectrometry data using singular value decomposition. *IGARSS'89 12th Canadian Symposium on Remote Sensing* (pp. 2069–2072).

Elmore, A. J., Mustard, J. F., Manning, S. J., & Lobell, D. B. (2000). Quantifying vegetation change in semiarid environments: Precision and accuracy of spectral mixture analysis and the normalized difference vegetation index. *Remote Sensing of Environment*, *73*, 87–102.

Flanagan, M., & Civco, D. L. (2001). Subpixel impervious surface mapping. *Proc. 2001 ASPRS Annual Convention, St. Louis, MO* (13 pp).

Getis, A. (1994). Spatial dependence and heterogeneity and proximal databases. In S. Fotheringham, & P. Rogerson (Eds.), *Spatial Analysis and GIS* (pp. 105–120). London: Taylor and Francis.

Gillespie, A. R., Smith, M. O., Adams, J. B., Willis, S. C., Fischer, A. F., & Sabol, D. E. (1990). Interpretation of residual images: Spectral mixture analysis of AVIRIS images, Owens Valley, California. *Proceedings of the 2nd Airborne Visible/Infrared Imaging Spectrometer (AVIRIS) Workshop, Pasadena, CA* (pp. 243–270).

Green, A. A., Berman, M., Switzer, P., & Craig, M. D. (1988). A transformation for ordering mutispectral data in terms of image quality with implications for noise removal. *IEEE Transactions on Geoscience and Remote Sensing*, *26*(1), 65–74.

Green, R. O., & Boardman, J. (2000). Exploration of the relationship between information content and signal/noise ratio and spatial resolution in AVIRIS data. In R. O. Green (Ed.), *Proceedings of the Ninth JPL Airborne Earth Science Workshop, Pasadena, CA* (pp. 195–206).

Herold, M., Gardner, M., Hadley, B., & Roberts, D. (2002). The spectral dimension in urban land cover mapping from high-resolution optical remote sensing data. *Proceedings of the 3rd Symposium on Remote Sensing of Urban Areas, June 2002, Istanbul, Turkey.*

Jackson, R. D. (1983). Spectral indices in n-space. *Remote Sensing of Environment*, *13*, 409–421.

Johnson, P. E., Smith, M. O., & Adams, J. B. (1985). Quantitative analysis of planetary reflectance spectra with principal components analysis. *Journal of Geophysical Research*, *90*, C805–C810.

Johnson, P. E., Smith, M. O., Taylor-George, S., & Adams, J. B. (1983). A semiempirical method for analysis of the reflectance spectra of binary mineral mixtures. *Journal of Geophysical Research*, *88*, 3557–3561.

Kauth, R. J., & Thomas, G. S. (1976). The tasseled cap—a graphic description of the spectral-temporal development of agricultural crops as seen by Landsat. *Proceedings of the Symposium on Machine Processing of Remotely Sensed Data* (pp. 4041–4051).

Kressler, F., & Steinnocher, K. (1996). Change detection in urban areas using satellite images and spectral mixture analysis. *Proceedings of the ISPRS.*

Kressler, F., & Steinnocher, K. (2000). Monitoring urban development using satellite images. *Proceedings of the Second International Symposium on Remote Sensing of Urban Areas, Regensburg, Germany.*

Liu, X., & Lathrop, R. G. (2002). Urban change detection based on an artificial neural network. *International Journal of Remote Sensing*, *23*(12), 2513–2518.

Madhavan, B. B., & Kubo, S. (2001). Appraising the anatomy and spatial growth of the Bangkok Metropolitan area using a vegetation–impervious–soil model through remote sensing. *International Journal of Remote Sensing*, *22*(5), 789–806.

Pagnutti, M., Ryan, R., Kelly, M., Holekamp, K., Zanoni, V., Thome, K., & Schiller, S. (2003). Radiometric characterization of IKONOS multispectral imagery. *Remote Sensing of Environment*, *88*, 52–67. (doi:10.1016/S0034-4257(03)00231-1)

Pech, R. P., Davies, A. W., Lamacraft, R. R., & Graetz, R. D. (1986). Calibration of Landsat data for sparsely vegetated semi-arid rangelands. *International Journal of Remote Sensing*, *7*, 1729–1750.

Phinn, S., Stanford, M., Scarth, P., Murray, A. T., & Shyy, P. T. (2002). Monitoring the composition of urban environments based on the vegetation–impervious surface–soil (VIS) model by subpixel analysis techniques. *International Journal of Remote Sensing*, *23*(20), 4131–4153.

Rashed, T., Weeks, J. R., Stow, D., & Fugate, D. (2002). Measuring temporal compositions of urban morphology through spectral mixture analysis: Toward a soft approach to change analysis in crowded cities. *Proceedings of the Third International Symposium on Remote Sensing of Urban Areas, Istanbul, Turkey, 11–13 June.*

Ridd, M. K. (1995). Exploring a V–I–S (Vegetation–Impervious Surface–Soil) model for urban ecosystem analysis through remote-sensing—Comparative anatomy for cities. *International Journal of Remote Sensing*, *16*(12), 2165–2185.

Roberts, D. A., Batista, G., Pereira, J., Waller, E., & Nelson, B. (1998). Change identification using multitemporal spectral mixture analysis: Applications in Eastern Amazonia. In C. Elvidge, & R. Lunetta (Eds.), *Remote Sensing Change Detection: Environmental Monitoring Applications and Methods* (pp. 137–161). Ann Arbor: Ann Arbor Press.

Roberts, D. A., Smith, M. O., & Adams, J. B. (1993). Green vegetation, nonphotosynthetic vegetation and soils in AVIRIS data. *Remote Sensing of Environment*, *44*, 255–269.

Ryan, R., Baldridge, B., Schowedgerdt, R., Choi, T., Helder, D., & Blonski, S. (2003). IKONOS spatial resolution and image interpretability. *Remote Sensing of Environment*, *88*, 37–51. (doi:10.1016/S0034-4257(03)00230-X)

Singer, R. B., & McCord, T. B. (1979). Large scale mixing of bright and dark surface materials and implications for analysis of spectral reflectance. *Journal of Geophysical Research*, 1835–1848.

Settle, J. J., & Drake, N. A. (1993). Linear mixing and the estimation of ground cover proportions. *International Journal of Remote Sensing*, *14*(6), 1159–1177.

Small, C. (2001a). Estimation of urban vegetation abundance by spectral mixture analysis. *International Journal of Remote Sensing*, *22*(7), 1305–1334.

Small, C. (2001b). Multiresolution analysis of urban reflectance. *Proceedings of the IEEE Workshop on Remote Sensing and Data Fusion of Urban Areas, 8–9 Nov. 2001, Rome, Italy.*

Small, C. (2001c). Spectral dimensionality of urban radiance. *Proceedings of 10th JPL Airborne Earth Science Workshop, NASA Jet Propulsion Laboratory, Pasadena, CA.*

Small, C. (2002a). A global analysis of urban reflectance. *International Journal of Remote Sensing* (In press).

Small, C. (2002b). Reflectance properties of pervious and impervious surfaces. *Proceedings of the ASPRS Pecora Land Remote Sensing Conference, Denver CO.*

Smith, M. O., Johnson, P. E., & Adams, J. B. (1985). Quantitative determination of mineral types and abundances from reflectance spectra using principal component analysis. *Journal of Geophysical Research*, *90, 792–804.*

Smith, M. O., Ustin, S. L., Adams, J. B., & Gillespie, A. R. (1990). Vegetation in deserts: I. A measure of abundance from multispectral images. *Remote Sensing of Environment*, *31*, 1–26.

Stefanov, W. L., Ramsey, M. S., & Christensen, P. R. (2001). Monitoring urban land cover change: An expert system approach to land cover classification of semiarid to arid urban centers. *Remote Sensing of Environment*, *77*(2), 173–185.

Wu, C. S., & Murray, A. T. (2003). Estimating impervious surface distribution by spectral mixture analysis. *Remote Sensing of Environment*, *84*(4), 493–505.

Wulder, M., & Boots, B. (1998). Local spatial autocorrelation characteristics of remotely sensed imagery assessed with the Getis statistic. *International Journal of Remote Sensing*, *19*(11), 2223–2231.

Zanoni, V., Stanley, T., Ryan, R., Pagnutti, M., Baldridge, B., Roylance, S., Snyder, G. L., & Lee, G. (2003). The joint agency commercial imagery evaluation (JACIE) team: Overview and IKONOS joint characterization approach. *Remote Sensing of Environment*, *88*, 17–22. (doi:10.1016/S0034-4257(03)00226-8)